ISSN 1063-7796, Physics of Particles and Nuclei, 2023, Vol. 54, No. 4, pp. 624–629. © Pleiades Publishing, Ltd., 2023.

Experimental Study of the $e^+e^- \to n\bar{n}$ Process at the VEPP-2000 Collider with the SND Detector

M. N. Achasov[a, b], A. Yu. Barnyakov[a, c], K. I. Beloborodov[a, b], A. V. Berdyugin[a, b], A. G. Bogdanchikov[a], A. A. Botov[a], T. V. Dimova[a, b], V. P. Druzhinin[a, b], L. V. Kardapoltsev[a, b], A. G. Kharlamov[a, b], A. A. Korol[a, b], D. P. Kovrizhin[a], A. S. Kupich[a, b], N. A. Melnikova[a], N. Yu. Muchnoy[a, b], A. E. Obrazovsky[a], E. V. Pakhtusova[a], K. V. Pugachev[a, b], S. I. Serednyakov[a, b, *], D. A. Shtol[a], Z. K. Silagadze[a, b], I. K. Surin[a], Yu. V. Usov[a], V. N. Zhabin[a, b], and V. V. Zhulanov[a, b]

[a] *Budker Institute of Nuclear Physics, Siberian Branch, Russian Academy of Sciences, Novosibirsk, 630090 Russia*

[b] *Novosibirsk State University, Novosibirsk, 630090 Russia*

[c] *Novosibirsk State Tecnical University, Novosibirsk, 630092 Russia*

**e-mail: seredn@inp.nsk.su*

Received October 20, 2020; revised June 15, 2021; accepted December 12, 2021

Abstract—In experiment at the VEPP-2000 e^+e^- collider the process $e^+e^- \to n\bar{n}$ has been studied in the energy from the threshold up to 2 GeV. To identify $n\bar{n}$ events the multichannel NaI(Tl) electromagnetic calorimeter of the SND detector was used. The measured $e^+e^- \to n\bar{n}$ process cross section is from 0.6 to 0.3 nb. The effective neutron timelike form factor is derived and compared with the proton form factor. The ratio $|G_E|/|G_M|$ of the neutron electric and magnetic form factor is obtained from the measured angular distribution and found to be between 1 and 2.

DOI: 10.1134/S1063779623040020

INTRODUCTION

The cross section of the nucleon-antinucleon pair production process depends on two functions G_E and G_M, called, respectively, the electric and magnetic timelike form factors of the nucleon:

$$\frac{d\sigma}{d\Omega} = \frac{\alpha^2\beta}{4s} \times \left[|G_M(s)|^2 (1+\cos^2\theta) + \frac{1}{\gamma^2}|G_E(s)|^2 \sin^2\theta \right], \quad (1)$$

where E_b is the beam energy, E is the center-of-mass (c.m.) energy, $sN_b^2 = E^2$, m_n is neutron mass, $\gamma = E_b/m_n$, $\beta = \sqrt{1-4m_n^2/s}$, α is the fine structure constant, and θ is the neutron production polar angle. The total cross section has the following form:

$$\sigma(s) = \frac{4\pi\alpha^2\beta}{3s}\left(1+\frac{1}{2\gamma^2}\right)|F(s)|^2, \quad (2)$$

where the function $F(s)$ is the so-called effective form factor:

$$|F(s)|^2 = \frac{2\gamma^2|G_M(s)|^2 + |G_E(s)|^2}{2\gamma^2+1}. \quad (3)$$

$F(s)$ is this function that is measured in most of $e^+e^- \to p\bar{p}$ and $n\bar{n}$ experiments.

The $e^+e^- \to n\bar{n}$ cross section near the threshold was measured previously in the FENICE [1], DM2 [2] and SND [3] experiments. The preliminary results from SND can be found in PhiPsi(2019) conference proceedings [4] and reported at the Nucleus 2020 conference [5]. One can found an article in ArXiv from BESIII Collaboration [6], where the $n\bar{n}$ production was measured in the energy above 2 GeV. In this work we report the current results on $e^+e^- \to n\bar{n}$ cross section in the SND experiment.

COLLIDER, DETECTOR, EXPERIMENT

The experiment was carried out at the VEPP-2000 e^+e^- collider [7] with SND detector [8]. VEPP-2000 operates in the c.m. energy range from 0.3 to 2.0 GeV. The collider has two collision regions, one of which is occupied by the SND detector. The collder luminosity varies from 10^{29} cm^{-2} s^{-1} at lower energy up to 5×10^{31} cm^{-2} s^{-1} at maximal energy. The beam energy spread above the $n\bar{n}$ threshold is about 0.7 MeV. The

beam energy is measured by laser Compton back-scattering system [9] with an accuracy of 0.05 MeV.

The SND (Spherical Neutral Detector) [8] is a general-purpose non-magnetic detector for a low energy collider (Fig. 1). It consists of a tracking system, an aerogel Cherenkov detector, a three-layer spherical highly segmented NaI(Tl) electromagnetic calorimeter (EMC) and a muon detector, consisting of scintillation counters and proportional tubes. The EMC is the main part of SND. It is intended to measure the electromagnetic shower energy and angles, but is also suitable to detect the neutrons and antineutrons. At the kinetic energy of several tens of MeV the annihilation length of antineutrons in NaI(Tl) does not exceed 15 cm [10], which is significantly lower than the EMC length (35 cm of NaI(Tl)). This leads to high absorbtion efficiency of produced antineutrons in the SND calorimeter.

The experimental data for the $n\bar{n}$ production study were taken in the energy range from the $n\bar{n}$ threshold up to 2 GeV. The collider instant luminosity during data taking runs varied in limits $1–4\times10^{31}$ cm^{-2} s^{-1}. The data have been recorded in 9 energy points in 2017 run and in 7 points in 2019 run. We also reanalyzed the 2012 run data in 5 energy points. The overall integrated luminosity of analysed data is about 40 pb^{-1}.

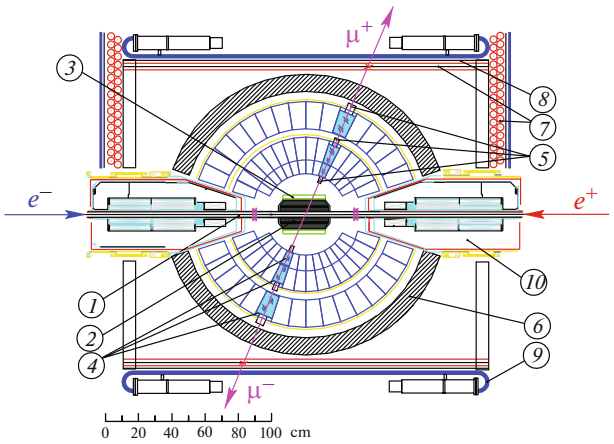

Fig. 1. SND detector, section along the beams: (*1*) beam pipe, (*2*) tracking system, (*3*) aerogel Cherenkov counters, (*4*) NaI (Tl) crystals, (*5*) vacuum phototriodes, (*6*) iron absorber, (*7*) proportional tubes, (*8*) iron absorber, (*9*) scintillation counters, (*10*) solenoids of collider.

BACKGROUNDS AND EVENTS SELECTION

The background in this experiment is of three types: physical, cosmic and beam-induced. The physical background arises from all e^+e^- annihilation processes, in particular, those with K_L meson in the final state. The cosmic background in contrary to the beam and physical backgrounds is evenly distributed in time. The beam background comes from the beam paricles interacting with the residial gas in the beam pipe, beam-beam single bremsstrahlung or internal beam scattering (Touschek effect).

The $n\bar{n}$ events are very different from events of other e^+e^- annihilation processes. Below 2 GeV the neutron from $n\bar{n}$ pair has a low energy and therefore gives low energy deposition in the calorimeter. So the signal from neutrons is not used in this analysis. The antineutron annihilates inside the EMC and produces pions, protons, neutrons with the total energy up to $2m_n$. Such an annihilation "star" in the EMC is a main sign of the neutron-antineutron event. Clusters of crystals with the energy deposition in EMC without accompanying charged tracks from the center are found in the reconstruction as photons. Typically, a $n\bar{n}$ event looks like a multiphoton event. A small part of the events contains off-center tracks in the drift chamber. In this analysis, the position of the calorimeter crystal with maximal energy deposition is taken as an estimate of the position of antineutron annihilation and used to determine the antineutron production angles, θ and φ.

Basing on the specifics of $n\bar{n}$ events and accociated background the following criteria are used in the events selection:

(1) No charged tracks in drift chamber area is found in an event.

(2) The muon veto signal (coincidence of external proportional tubes and scintillation counters) is required.

(3) The most energetic reconstructed photon in an event has the transverse energy profile (parameter $xi2g > -2.5$), not consistent with the electromagnetic shower profile [11].

(4) The large unbalanced total event momentum is measured in the calorimeter ($P_{EMC} > 0.4E_b$).

(5) To reject the beam-induced and cosmic background, the total energy deposition in EMC is required to be within the limits $E_b < E_{EMC} < 2$ GeV.

(6) To study the systematics in the detection efficiency, a loosened cut on the total EMC energy is used: $E_{EMC} > 0.7E_b$.

(7) To reduce the cosmic background, the events with cosmic track, reconstructed in EMC are rejected. In addition, the events with cosmic showers in EMC with the profile described by the function *shcosm* [3], are removed by the cut $shcosm > 0.4$.

(8) The cosmic background is additionally suppressed by the condition on the energy E_3 in the third layer of the calorimeter: $E_3 < 0.75E_b$.

(9) The reconsructed antineutron production angle lies within the sensitive EMC aperture $36° < \theta < 144°$.

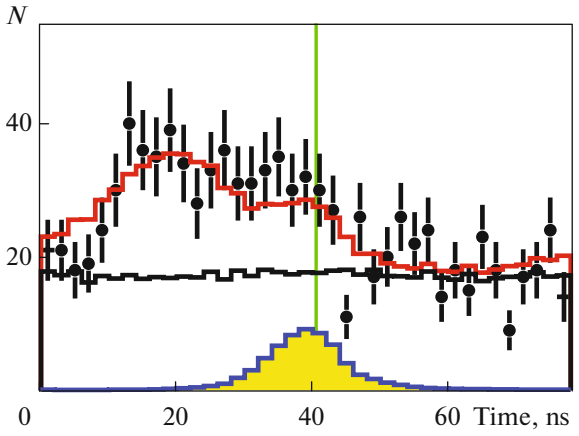

Fig. 2. The distribution between the event time and the beam collision time at E_b = 940.2, 940.8, 942 MeV in 2017 run. The black histogram represents cosmic background. The filled yellow histogram shows the expected beam background distribution. The red histogram is the result of the fit described in the text. The vertical line indicates the position of zero delay between the trigger and the beam collision.

The general selection condition (let's call it Tr1) is written in the following form: Tr1 = $1\times2\times3\times4\times5\times6\times7\times8\times9$, where the numbers correspond to the itemized conditions listed above.

As a result of applying the base condition Tr1 to the data, the selected events number N was reduced to the level $N/L \sim 200$ events per inverse picobarn of integrated luminosity L, what makes possible the subsequent analysis of data.

DETERMINIG THE NUMBER OF $n\bar{n}$ EVENTS

Due to the low antineutron velosity $v_n < c$ the $n\bar{n}$ signal in EMC is delayed with respect to the typical e^+e^- annihilation events, e.g., events from the $e^+e^- \to \gamma\gamma$ process, by about 10 ns. Such a delay is a good indication of a desired $n\bar{n}$ event. In analysis of 2017 data we measured the delay between the EMC first level trigger and the r.f. phase with a rather poor time resolution of about 6 ns. The condition Tr1 described above is used to select $n\bar{n}$ events. The data time distribution for different energy intervals are shown in Fig. 2. The wide peak on the left in Fig. 2 at the energy close to the the $n\bar{n}$ threshold cooresponds to the awaited $n\bar{n}$ signal smeared with the experimental $e^+e^- \to \gamma\gamma$ time spectrum. The cosmic distribution is uniform over time. The beam background is concentrated around the vertical line, corresponding to the beam collisions time, and shown separately below. With increasing energy, the $n\bar{n}$ signal delay decreases and the peak approaches the zero time. Next, the data time distribution is fitted by a sum of the MC $n\bar{n}$, cosmic and beam-background time spectra:

$$F(t) = N_{n\bar{n}}H_{n\bar{n}}(t) + N_{\rm csm}H_{\rm csm}(t) + N_{\rm bg}H_{\rm bg}(t), \quad (4)$$

where histograms $H_{n\bar{n}}$, $H_{\rm csm}$ and $H_{\rm bg}$ are normalized time distributions of MC $n\bar{n}$ signal, cosmic and beam background, $N_{n\bar{n}}$ and $N_{\rm csm}$ are the free fit parameters, corresponding to the total number of $n\bar{n}$ signal and cosmic events. The beam background in 2017 run data is not fitted, the number of background events is taken proportional to the luminosity $N_{\rm bg} \simeq L\sigma_{\rm bg}$ at a given energy point. A special study at the energy E_b = 900–939 MeV below the $n\bar{n}$ threshold shows that the background detection cross section $\sigma_{\rm bg}$ does not depend on the beam energy and its value is 12 ± 2 pb under the Tr1 selection condition. The high statistics cosmic histogram $H_{\rm csm}$ is measured with a cosmic trigger that includes the coincidence of the external muon system and the energy deposition ($E_{\rm EMC} > 0.7$ GeV) in the calorimeter. The red solid histogram in Fig. 2 describes the total sum of signal and background contributions. As a result of the fit, we determine the number $N_{n\bar{n}}$ of $n\bar{n}$ events in each energy point. In total, about 1000 $n\bar{n}$ data events are found in the 2017 run. Using the same technique we reanalyzed the 2012 data and selected 300 $N_{n\bar{n}}$ events in 5 energy points.

In 2019 run the time measurement technique in EMC was significantly improved [12]. The signal from the EMC photodetector, shaped with an integration time of about 1 μs, is digitized by a flash ADC with a 36 MHz sampling frequency and amplitude and time of the signal are calculated. The EMC time resolution measured using $e^+e^- \to \gamma\gamma$ events is found to be 0.8 ns. This is nearly an order of magnitude lower than in the 2017 run. The event time in a calorimeter counter is defined as a difference between the time from the preliminary measured time of $e^+e^- \to e^+e^-$ process and a counter time. Then the $n\bar{n}$ event time is calculated as an averaged time over all EMC counters with energy deposition larger than 30 MeV with weights proportional to their energy deposition.

The data time distribution for selected events is shown in Fig. 3 at the beam energy E_B = 945 MeV. The delayed $n\bar{n}$ events are located to the right. It can be seen that with increasing energy, the signal delay decreases and the $n\bar{n}$ peak shifts to the zero time. Similar to the run 2017, the time distribution consists of the uniform cosmic distribution, the beam background distribution peaked near zero time and a wide $n\bar{n}$ distribution located between 3 and 15 ns. The width of the $n\bar{n}$ spectrum is determined by the spread of the antineutron annihilation points—from the wall of the beam pipe to the rear wall of the calorimeter. The possible difference between the data and MC time spectra can be explained by the discrete structure of the calorimeter, which is reproduced slightly differ-

ently in data and simulation, but this difference has practically no effect on the final results. This remark also applies to data from 2012 and 2017. The time distribution in Fig. 3 is fitted by the function Eq. (4) with the beam background taken as a free fit parameter. This became possible, in contrast to the 2017 run data, due to the fact that the signal and background spectra differ in shape and location. Similar to the 2017 data, the cosmic spectrum H_{csm} is measured with the cosmic trigger and the shape of the beam background H_{bg} is measured at energies up to the $n\bar{n}$ threshold. As a result of the fit we determine the number of $n\bar{n}$ events in each energy point. The calculated detection cross section for the beam background σ_{bg}, as expected, turned out to be generally independent of the energy, its value is about 12 pb. In total, about 1500 $n\bar{n}$ events are found in the 2019 run.

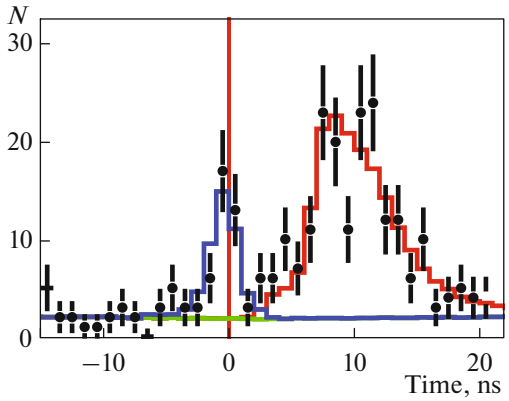

Fig. 3. The distribution between the beam collision time and the event time at E_b = 945 MeV in 2019 run. The green line represents the cosmic background. The blue histogram shows the beam background. The red histogram is the MC $n\bar{n}$ time distribution. The vertical line indicates the position of zero delay time.

DETECTION EFFICIENCY

The detection efficiency ε is calculated using Monte Carlo (MC) simulation. The simulation includes emission of an additional photon by initial electron and positron and takes into account the c.m. energy spread, which is about 1 MeV. The $\cos\theta$ distribution in Eq. (1) is taken to be uniform in the simulation, which close to the threshold approximately corresponds to $|G_E| = |G_M|$. The simulation also takes into account spurious photons and charged tracks arising from the beam background. They are simulated by using special background events recorded during data taking with a random trigger. These events are superimposed on the simulated $n\bar{n}$ events. The detector response is simulated with the GEANT4 toolkit [13], release 10.5. Under selection Tr1 the detection efficiency ϵ smoothly depends on the beam energy and polar angle in limits of the detector aperture. Its average value is about 20%.

The correctness of the detection efficiency is a matter of particular importance. Comparison of data and MC, for example, for the total energy deposition in the calorimeter shows a satisfactory agreement between the data and MC. To check it on a larger scale using data from 2019 run, we have significantly weakened the selection condition, which led to an increase in the detection efficiency up to 50%. This led to a significant increase in the cosmic and beam background, so the number of events was obtained with a much larger error. The resulting correction $R_{19} = 1.10 \pm 0.10$ is practically independent of energy and is applied to the 2017 and 2012 data. The quoted error in R_{19} correction is statistical. The additional systematics is defined by the variation of the beam background in magnitude and shape and varies in limits 3–9%.

About 10% of $n\bar{n}$ events give tracks in the SND drift chamber. Their origin is not related to the beam collision point. The main background for $n\bar{n}$ events with tracks comes from $e^+e^- \to p\bar{p}$ process, with antiprotons annihilation in the material before the drift chamber. The requirement of no tracks in an events reduces this background to negligible level. We calculated the joint correction from the condition for no charged tracks in an event (item 1' in Section) and the restriction on the detection solid angle (item 9' in Section). The found correction turned out to be independent of the beam energy and amounted to 0.985 ± 0.015.

There are also additional sources of errors—calorimeter calibration 2.5%, radiative corrections 2–5%, luminosity measurement accuracy 2%.

In total, the systematic error in measuring the cross section is estimated at 15%.

THE $e^+e^- \to n\bar{n}$ CROSS SECTION

The Born cross section σ_0 for the process $e^+e^- \to n\bar{n}$ is related to the experimental data as follows

$$\sigma_{vis} = N/(\varepsilon L) = \sigma_0(1+\delta);$$
$$\sigma_{vis} = \int_{\Delta E} P(E',E)dE' \int_0^{x_{max}} W(s,x)\sigma_0(s(1-x))dx, \quad (5)$$

where σ_{vis} is so called visible cross section, $1+\delta$ is the radiative correction factor, N is the number of $n\bar{n}$ events, obtained by fitting the experimental time spectra, ε is the detection efficiency, L is integrated luminosity, $P(E',E)$ is a Gaussian function describing the beam energy spread, $W(s,x)$ is the radiator function [14], describing emission of photons by initial electrons and positrons, $x = \omega/E_b$, ω is radiative photon energy. The radiative correction $1+\delta$ is calculated

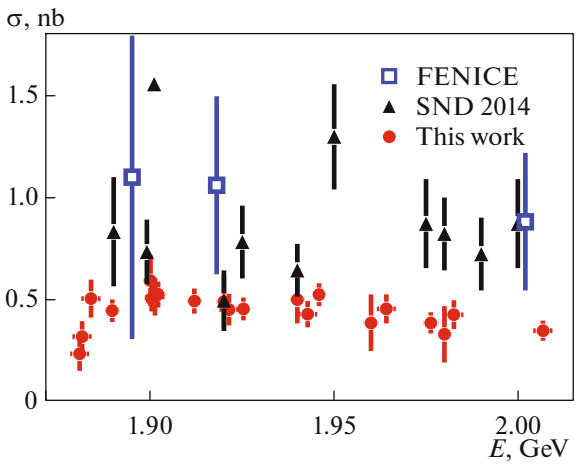

Fig. 4. The $e^+e^- \to n\bar{n}$ cross section measured in this work (solid circles) compared with the previous FENICE [1] (empty squares) and SND [3] (filled triangles) measurements. Results are preliminary. Only statistical error are shown.

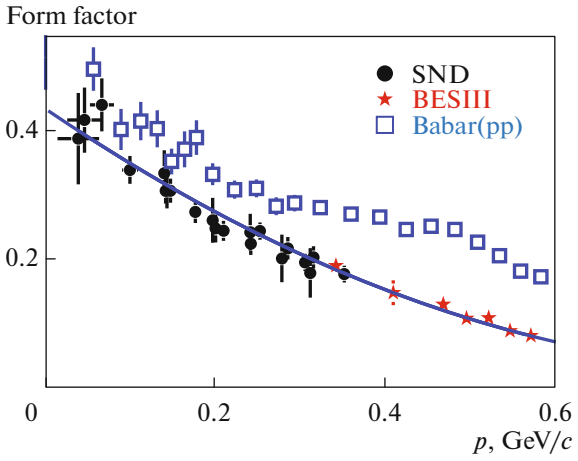

Fig. 5. The neutron effective form factor obtained in this work (solid black circles), compared with BESIII [6] neutron form factor (red atars) and proton form factor measured by BABAR [16] (empty squares). Results are preliminary.

according to the Eq. (5) taking into account the beam energy spread and measured dependence of the cross section on energy. Its value varies with energy from 0.7 to 0.9.

The $e^+e^- \to n\bar{n}$ cross section calculated with the base condition *Tr*1 using Eq. (5), is corrected by the factor R_{19} and other corrections listed in Section 9. The full data on the cross section σ_0 from 2012, 2017 and 2019 runs are shown in Fig. 4 together with previous measurements in the energy up to 2 GeV. The errors are statistical. On average, σ_0 is about 0.4 nb, what is considerably lower than in data from FENICE [1] and SND [3]. On the other hand, at the maximum available energy of our experiment $E = 2$ GeV, our cross section result $\sigma_0 = 0.3$ nb is in good agreement with the preliminary data of the BES3 experiment [6].

As for prediction it is worth mentioning the article [15], where the cross section ≃0.4 nb is predicted near the threshold at $E_b < 950$ MeV. True, with increasing the energy, their prediction for the cross section diverges from our data. The $e^+e^- \to n\bar{n}$ cross section obtained in this work superecedes our previous results SND [3]. In that work, the contribution of the beam and physical background was underestimated.

THE EFFECTIVE NEUTRON FORM FACTOR AND $|G_E/G_M|$ RATIO

The effective neutron form factor is calculated from the measured cross section using Eq. (2). The form factor values as a function of the neutron momentum are plotted in Fig. 5 together with BESIII results at higher energy. The proton form factor from the BABAR experiment [16] is shown for comparison as well. One can see that near the threshold both neutron and proton form factor are close to each other within the measurement errors, but with energy increase the neutron form factor becomes considerably lower. The asymptotic prediction for nucleons form factors $|F_n| = |F_p|/2$ [17] seems to start working at $E > 2$ GeV. To derive the $|G_E|/|G_M|$ ratio, following to Eq. (1), the mesured $\cos\theta$ distribution is fitted with the function:

$$F(\cos\theta) = N((1-\alpha)H_M + \alpha H_E), \qquad (6)$$

where H_M and H_E are the histograms, describing the contributions of the $|G_M(s)|^2$ and $|G_E(s)|^2$ terms in Eq. (1), respectively, obtained using simulation, N is proportional to the total number of events. The fit parameter α describes the relative contribution of $|G_M(s)|^2$ and $|G_E(s)|^2$ terms. The $|G_E|/|G_M|$ ratio is determined as follows:

$$|G_E|/|G_M| = \gamma\sqrt{(\alpha/(1-\alpha))}, \qquad (7)$$

where $\gamma = E_b/m_n$. The values of $|G_E|/|G_M|$ in three energy intervals are shown in Fig. 6. Our data do not contradict the condition $|G_E|/|G_M| = 1$ at the very threshold. Despite the large measurement errors, there is a tendency seen to increase the $|G_E|/|G_M|$ ratio with energy. A similar picture in this value is observed for the proton [16]. The rise in the value of $|G_E|/|G_M|$ leads to a increase in the detection efficiency ε, so at $|G_E|/|G_M| = 1.5$ the correction to the ε is 1.06 ± 0.03, This correction is taken into account when calculating the final cross section.

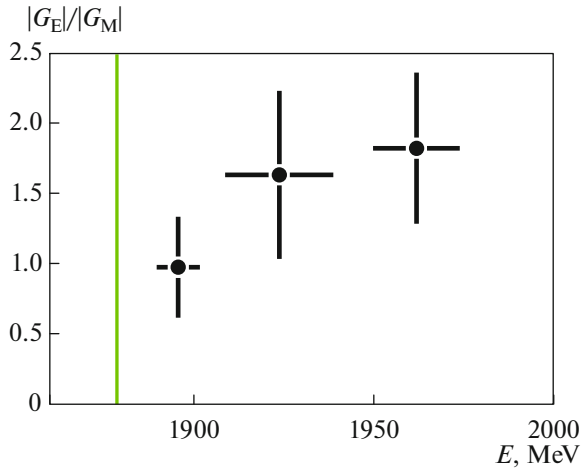

Fig. 6. The measured ratio $|G_E|/|G_M|$ for neutron timelike form factor for 2019 run data. The vertical line corresponds to the nucleon production threshold. Results are preliminary.

CONCLUSIONS

The experiment to measure $e^+e^- \to n\bar{n}$ cross section has been carried out with the SND detector at the VEPP-2000 e^+e^- collider in the energy region from the nucleon-antinucleon threshold up to 2 GeV. The $e^+e^- \to n\bar{n}$ cross section value is measured to be about 0.4 nb. This value is cosiderably lower than in the previous measurements. From the measured cross section the neutron effective timelike form factor has been extracted. Its value is found to be close to the proton form factor at the threshold but becomes lower with the increase of energy. Using the measured antineutron production $\cos\theta$ distribution the ratio of the electric and magnetic neutron form factors $|G_E|/|G_M|$ is obtained.

FUNDING

This work is supported by the Russian Foundation for Basic Research, grant 20-02-00347A.

CONFLICT OF INTEREST

The authors declare that they have no conflicts of interest.

REFERENCES

1. A. Antonelli et al. (FENICE Collab.), "The first measurement of the neutron electromagnetic form factors in the time-like region," Nucl. Phys. B **517**, 3–35 (1998). https://doi.org/10.1016/S0550-3213(98)00083-2
2. M. E. Biagini et al. (DM2 Collab.), "U-spin considerations to guess the unknown time-like neutron form factors," Z. Phys. C **52**, 631 (1991). https://doi.org/10.1007/BF01562337
3. M. N. Achasov et al. (SND Collab.), "Study of the process $e^+e^- \to n\bar{n}$ at the VEPP-2000 e^+e^- collider with the SND detector," Phys. Rev. D **90**, 112007 (2014). https://doi.org/10.1103/PhysRevD.90.112007
4. V. P. Druzhinin and S.I. Serednyakov (SND Collab.), "Measurement of the $e^+e^- \to n\bar{n}$ cross section with the SND detector at the VEPP-2000 collider," EPJ Web Conf. **212**, 07007 (2019). https://doi.org/10.1051/epjconf/2019212007007
5. S. I. Serednyakov (SND Collab.), "Measurement of the neutron time-like electromagnetic form factor at the VEPP-2000 e^+e^- collider with the SND detector," *in Proceedings of 30th "Nucleus-2020" Conference, St. Petersburg, 2020.* https://indico.cern.ch/event/839985/ 11-17.
6. M. Ablikim et al. (BESIII Collab.), "New features in the electromagnetic structure of the neutron," arXiv: 2103.12486v3 [hep-ex].
7. P. Yu. Shatunov et al., "Status and perspectives of the VEPP-2000," Part. Nucl. Lett. **13**, 995—1001 (2016). https://doi.org/10.1134/S154747711607044X
8. M. N. Achasov et al., "First experience with SND calorimeter at VEPP-2000 collider," Nucl. Instrum. Methods Phys. Res., Sect. A **598**, 31–33 (2009). https://doi.org/10.1016/j.nima.2008.08.012
9. E. V. Abakumova et al., "A system of beam energy measurement based on the Compton backscattered laser photons for the VEPP-2000 electron-positron collider," Nucl. Instrum. Methods Phys. Res., Sect. A **744**, 35–40 (2014). https://doi.org/10.1016/j.nima.2014.01.020
10. M. Astrua et al., "Antineutron-nucleus annihilation cross sections below 400 MeV/c," Nucl. Phys. A **697**, 209–224 (2002). https://doi.org/10.1016/S0375-9474(01)01252-0
11. A. V. Bozhenok et al., "Transverse energy profile of electromagnetic shower," Nucl. Instrum. Methods Phys. Res., Sect. A **379**, 507–508 (1996). https://doi.org/10.1016/0168-9002(96)00548-7
12. M. N. Achasov et al., "Time resolution of the SND electromagnetic calorimeter," J. Instrum. **10**, T06002 (2015). https://doi.org/10.1088/1748-0221/10/06/T06002
13. S. Agostinelli et al. (GEANT Collab.), "GEANT4 -a simulation toolkit," Nucl. Instrum. Methods Phys. Res., Sect. A **506**, 250–303 (2003). https://doi.org/10.1016/S0168-9002(03)01368-8
14. M. Benayoun et al., "Spectroscopy at B-factories using hard photon emission," Mod. Phys. Lett. A **14**, 2605–2614 (1999). https://doi.org/10.1142/S021773239900273X
15. A. I. Milstein and S. G. Salnikov, "Fine structure of the cross section of e^+e^- annihilation near the threshold of $p\bar{p}$ and $n\bar{n}$ production," Nucl. Phys. A **977**, 60—68 (2018) https://doi.org/10.1016/j.nuclphysa.2018.06.002
16. J. P. Lees et al. (BABAR Collab.), "Study of $e^+e^- \to n\bar{n}$ via initial-state radiation at BABAR," Phys. Rev. D **87**, 092005 (2013). https://doi.org/10.1103/PhysRevD.87.092005
17. V. L. Chernyak and A. R. Zhitnitsky, "Asymptotic behaviour of exclusive processes in QCD," Phys. Rept. **112**, 173 (1984). https://doi.org/10.1016/0370-1573(84)90126-1